Pergamon

Int. J. Heat Mass Transfer. Vol. 38, No. 13, pp. 2333–2342, 1995

0017-9310/95 $9.50+0.00

0017-9310(94)00364-5

Effects of wall transpiration on mixed convection in a radial outward flow inside rotating ducts

WEI-MON YAN

Department of Mechanical Engineering, Hua Fan College of Humanities and Technology, Shih Ting, Taipei, Taiwan 22305, Republic of China

(*Received* 19 *July* 1994 *and in final form* 5 *December* 1994)

Abstract—The present work treats the transport phenomena in a radial outward flow inside rotating ducts with rotation-induced buoyancy and wall transpiration effects. Using the vorticity–velocity method, the three-dimensional Navier–Stokes equations and the energy equation were solved simultaneously. Predicted results are presented for air flowing in a rectangular duct over a wide range of governing parameters. In this work, both the thermal boundary conditions of uniform wall temperature (UWT) and uniform heat flux (UHF) are considered. The results disclose that the axial variations of the peripherally averaged friction factor and Nusselt number are closely related to the emergence, disappearance, growth and decay of the rotation-induced secondary vortices. The Nu is enhanced with an increase in the rotation number Ro. Predicted results also show that near the entrance, the fRe increases with an increase in the wall Reynolds number Re_w. But as the flow goes downstream, the fRe decreases with Re_w. Additionally, the fRe and Nu for the UWT case are lower than those for the UHF case near the inlet but surpass them downstream.

INTRODUCTION

The heat transfer and fluid flow in porous-walled passages is of importance in many engineering applications. The porous-walled ducts are used in heat exchangers, solar energy collectors, transpiration cooling of gas-turbine blades, combustion chambers, exhaust nozzles and porous-walled flow reactors. Among these, the transpiration cooling of rotating turbine blades is to prevent the blade failure due to the combination of high thermal loads and centrifugal stressing. In transpiration cooling, the coolant air transpires through the porous wall and carries the heat away. It has been proved that the transpiration cooling is the most effective one among the turbine cooling. The high efficiency stems from two mechanisms: (1) the heat is carried away by the coolant air through the duct and (2) the relatively cool (compared to the external hot gas stream) fluid transpired through the porous skin forms a high thermal-resistance protection layer over the blade. In an engineering point of view, the transpiration cooling in turbine rotor blades can be modeled as the heat convection in radially rotating ducts with wall-transpiration [1, 2]. Flow and heat transfer mechanisms in a radially rotating channel are very complicated due to the presence of Coriolis-induced secondary flow and rotation-induced buoyancy effects. The geometric parameter (aspect ratio) can also influence the growth and the strength of the secondary flow and therefore is a critical factor in heat transfer mechanism. Additionally, in a transpiration cooling duct wall-transpiration effect should be considered and the convection process becomes more complicated.

A vast amount of work, both theoretical and experimental, exists in the literature to study the flow and heat transfer in porous-walled passages without rotation, as is evident in a recent review by Soong [2]. Only those relevant to the present work are briefly reviewed here. A similarity solution was obtained by Berman [3] and Donoughe [4] for a two-dimensional duct with wall suction and injection. Based on the assumption of fully developed flow, they successfully solved the governing equations of flow field for small wall transpiration by using the perturbation technique. Studies on developing flow in porous-walled ducts with suction and injection effects were carried out by Raithby and Knudsen [5] and Sorour *et al.* [6]. The effects of wall transpiration on the fully-developed heat transfer were investigated extensively by Carter and Gill [7], Terrill [8] and Kinney [9]. Among these studies, the solutions were limited to either a small wall-suction or only valid for the fully-developed flow regime. The thermal entrance heat transfer with fully-developed velocity distributions in porous ducts was carried out by Pederson and Kinney [10] and Raithby [11]. In refs. [10, 11], various thermal boundary conditions were investigated. The numerical analyses for the simultaneously developing flow and temperature fields in the entrance region of porous ducts were examined by Doughty and Perkins [12], Rhee and Edwards [13] and Fagher [14]. Recently, Hwang *et al.* [15] presented a numerical study of forced convection heat transfer and fluid flow

NOMENCLATURE

A cross-sectional area of the rectangular duct [m^2]
a, b width and height of the rectangular duct, respectively [m]
D_e equivalent hydraulic diameter [4A/S]
f friction factor, $2\tau_w/(\rho\bar{w}_0^2)$
Gr_Ω rotational Grashof number, $(\Omega^2 D_e)\beta\Delta T D_e^3/\nu^2$
$\bar{h}$ peripherally averaged heat transfer coefficient [W m^{-2} K^{-1}]
M, N number of grid points in the X and Y directions, respectively
m mth iteration
n dimensionless outward normal direction to the duct wall
Nu peripherally averaged Nusselt number, $\bar{h}D_e/k$
p pressure [kPa]
$\bar{P}, p_m$ dimensionless and dimensional cross-sectional mean pressure, $\bar{P} = \bar{p}/(\rho\bar{w}_o)$
P' perturbation pressure about the mean pressure $\bar{P}$
Pr Prandtl number, ν/α
q''_w wall heat flux [W m^{-2}]
Re inlet Reynolds number of the gas stream, $\bar{w}_o D_e/\nu$
Re_w wall Reynolds number, $u_w D_e/\nu$
Ro rotation number, $\Omega D_e/\bar{w}_o$
S circumference of cross section [m]
T temperature [K]
T_o inlet temperature [K]
T_w wall temperature [K]
u, v, w velocity components in the X, Y and Z directions, respectively [m s^{-1}]
U, V, W dimensionless velocity components in the X, Y and Z directions, respectively, $U = u/\bar{w}_o$, $V = v/\bar{w}_o$, $W = w/\bar{w}_o$
u_w, U_w dimensional and dimensionless suction velocity at porous wall, $u_w/\bar{w}_o$
$\bar{W}$ dimensionless local mean velocity in axial direction, $\bar{W} = \bar{w}/\bar{w}_o$
$\bar{w}_o$ mean axial velocity at the inlet [m s^{-1}]
x, y, x rectangular coordinates [m]
X, Y, Z dimensionless rectangular coordinates, $X = x/D_e$, $Y = y/D_e$, $Z = z/D_e$
z_o, Z_o dimensional and dimensionless distance from the axis of rotation to inlet, respectively.

Greek symbols

α thermal diffusivity [m^2 s^{-1}]
β coefficient of thermal expansion
γ aspect ratio of a rectangular duct, a/b
ΔT_c characteristic temperature difference, $(T_w - T_o)$ for UWT; $(q''_w D_e/k)$ for UHF
θ dimensionless temperature, $(T - T_o)/\Delta T_c$
ν kinematic viscosity [m^2 s^{-1}]
ξ dimensionless vorticity in axial direction
ρ density [kg m^{-3}]
τ_w wall shear stress [kPa]
Ω angular velocity of rotation [s^{-1}].

Subscripts

b bulk fluid quantity
o condition at inlet
w value at wall.

Superscript

$\bar{}$ averaged value.

in the entrance region of a square duct with one-walled injection and suction. They found that the wall transpiration has a significant impact on the heat transfer and fluid flow in the entrance region of porous ducts.

The effects of Coriolis force on the fluid flow and heat transfer in rotating ducts were reviewed below. Mori and Nakayama [16] theoretically analyzed the laminar fully developed heat transfer in a radially rotating pipe. They assumed that the flow consisted of a central core and a relatively thin boundary layer in the immediate vicinity of the wall. It was shown that the Coriolis force caused a significant enhancement in both friction factor and Nusselt number. Fully developed laminar flow and heat transfer in radially rotating rectangular ducts was examined numerically by Hwang and Jen [17]. The friction factor and Nusselt number were reported for a large range of parameters, and showed qualitative agreement with experiment. In ref. [17], the effect of axial fluid conduction was also included. In the experimental study on the heat transfer in rotating ducts, Morris and Ayhan [18] and Morris [19] showed that the centrifugal-buoyancy effect has an advantage effect on the heat transfer for radially inward flow but an adverse effect for radially outward flow. This class of flows has an analogy to mixed convection, buoyancy-aiding and opposing, in a gravitational field. Similar trends were also found by Siegel [20] and Harasgama and Morris [21]. Experimental study on convective heat transfer in radially rotating ducts was conducted by Soong *et al.* [22] and Wagner *et al.* [23]. Rotation

was found to affect the heat transfer coefficients differently at different locations inside the coolant passages. Taslim *et al.* [24] experimentally investigated the heat transfer in a rotating channel with ribbed walls. The effect of uneven wall temperature on the local heat transfer coefficient in a radially rotating square duct with radial outward flow was examined by Han and Zhang [25]. It was disclosed that the local uneven wall temperature created the local buoyancy forces, which changed the effect of the rotation. Recently, the experimental measurements on the convective heat transfer in rotating serpentine passage were carried out by Wagner *et al.* [26] and Fann *et al.* [27]. Developing flow and heat transfer in radially rotating rectangular ducts was investigated numerically by Jen *et al.* [28] and Jen and Lavine [29]. In their studies, the rotation-induced buoyancy was neglected. The studies of refs. [28, 29] were extended by Fann and Yang [30] and Fann *et al.* [31]. They found that the vortex numbers were varied with the geometry, throughflow rate, rotation number, and location along the channel. In the above studies, no wall-transpiration effects are included.

It is noted that that study of flow and heat transfer in rotating ducts with wall transpiration has not received sufficient attention. Soong and Hwang [32, 33] solved the flow and heat transfer in two-dimensional semiporous-walled channel in the presence of rotation by the similarity method. In their studies, the height–width aspect ratio was assumed to be small in order to neglect the side effect. From an engineering point of view, only ducts with very small height–width aspect ratios can be treated as parallel plates. Also, many applications are known to have a moderate or high aspect aspect ratio. Recently, Yan [34] numerically examined the effects of wall transpiration on forced convection heat transfer in radially rotating rectangular ducts subjected to a uniform wall temperature. In his study, the rotation-induced centrifugal buoyancy is neglected. In fact, in high rotation rate/or high wall-to-fluid temperature difference in a rotating duct, the centrifugal buoyancy may play a very critical role in the flow and heat transfer characteristics. This motivates the present study which is to examine the mixed convection flow and heat transfer in a radial outward flow inside rotating rectangular ducts with wall-transpiration effects. Both the thermal boundary conditions of uniform wall temperature (UWT) and uniform heat flux (UHF) are considered in this work.

ANALYSIS

Figure 1 shows a rectangular duct rotating at a constant angular speed Ω about an axis normal to the main flow direction. The axis of rotation lies at a distance z_o away from the channel entrance. The main stream flows along the duct axis and blades out through the porous wall at a uniform transpiration velocity u_w. In this work, a uniform axial velocity $\bar{w}_o$ and a constant temperature T_o are imposed at the entrance $z = 0$. The duct walls are subjected to either uniform wall temperature T_w or uniform heat flux q''_w. The u, v and w are the velocity components in the x, y and z directions, respectively. The flow is assumed to be laminar and steady. Since the rotation-induced buoyancy becomes pronounced in the presence of the high rotational speed, Boussinesq approximation is invoked to allow for a linear variation of density with temperature in centrifugal buoyancy terms. Gravitational effect is relatively small and is neglected in the present study.

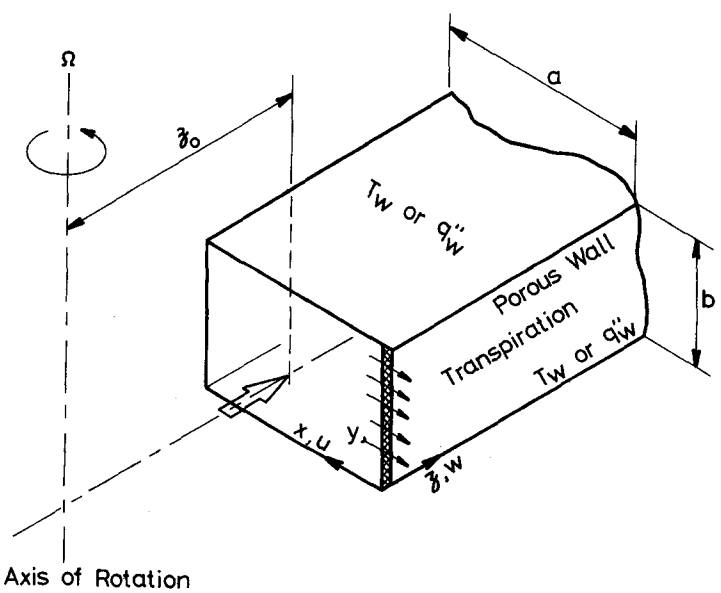

Fig. 1. Schematic diagram of the physical system.

Governing equations

The pressure gradient and centrifugal force terms in the x- and z-directions are $-\partial p/\partial x+\rho\Omega^2 x$ and $-\partial p/\partial z+\rho\Omega^2(z_o+z)$, respectively. By defining a pressure function p_m and $p_m = p-p_o$, where p_o denotes the flow pressure at the inlet, and rearranging the pressure and centrifugal force terms, one has

$$-\partial p/\partial x+\rho\Omega^2 x = -\partial p_m/\partial x-\rho\beta(T-T_o)\Omega^2 x \tag{1a}$$

$$-\partial p/\partial z+\rho\Omega^2(z_o+z) = -\partial p_m/\partial z-\rho\beta(T-T_o)\Omega^2(z+z_o). \tag{1b}$$

For convenience in implementing the axial marching integration, the pressure function $p_m(x, y, z)$ is split into a cross-sectional average $\bar{p}(z)$ driving the main flow and a perturbation pressure $p'(x, y)$ driving the cross stream flow, namely

$$p_m = \bar{p}(z)+p'(x, y). \tag{2}$$

This "pressure uncoupling" follows the parabolic-flow practice and, together with the assumption that neither momentum nor heat is diffused in the axial direction by an order of magnitude analysis, permits a marching-integration procedure [35].

Consider the above pressure splitting and perform a proper scaling procedure, the problem can be formulated by the following dimensionless vorticity–velocity formulation [30, 31, 34]:

$$\partial^2 U/\partial X^2+\partial^2 U/\partial Y^2 = \partial\xi/\partial Y-\partial^2 W/\partial X\,\partial Z \tag{3}$$

$$\partial^2 V/\partial X^2+\partial^2 V/\partial Y^2 = -\partial\xi/\partial X-\partial^2 W/\partial Y\,\partial Z \tag{4}$$

$$\begin{aligned} &U\,\partial\xi/\partial X+V\,\partial\xi/\partial Y+W\,\partial\xi/\partial Z\\ &\quad+\xi(\partial U/\partial X+\partial V/\partial Y)+(\partial W/\partial Y\cdot\partial U/\partial Z\\ &\quad-\partial W/\partial X\cdot\partial V/\partial Z)+2Ro\cdot\partial W/\partial Y\\ &=(\partial^2\xi/\partial X^2+\partial^2\xi/\partial Y^2)/Re-(Gr_\Omega/Re^2)X\,\partial\theta/\partial Y \end{aligned} \tag{5}$$

$$\begin{aligned} &U\,\partial W/\partial X+V\,\partial W/\partial Y+W\,\partial W/\partial Z\\ &\quad=-\mathrm{d}\bar{P}/\mathrm{d}Z+(\partial^2 W/\partial X^2+\partial^2 W/\partial Y^2)/Re\\ &\qquad+2Ro\cdot U-(Gr_\Omega/Re^2)\theta(Z_o+Z) \end{aligned} \tag{6}$$

$$\begin{aligned} &U\,\partial\theta/\partial X+V\,\partial\theta/\partial Y+W\,\partial\theta/\partial Z\\ &\quad=(\partial^2\theta/\partial X^2+\partial^2\theta/\partial Y^2)/(Pr\cdot Re) \end{aligned} \tag{7}$$

where $\xi = \partial U/\partial Y-\partial V/\partial X$ is the axial vorticity.

Equations (3)–(7) are used for solving U, V, W, ξ and θ. An additional constraint for deduction of the pressure gradient in the axial momentum equation can be derived from the overall mass balance at every axial location. This can be expressed as

$$\bar{W} = 1-(Re_w/Re)[2/(1+\gamma)]Z. \tag{8}$$

The problem is subjected to the following boundary conditions:

$$W = 1\ U = V = \xi = \theta = 0 \text{ at the entrance } Z = 0 \tag{9a}$$

$$U = V = W = 0 \quad \theta = 1 \text{ (UWT)}$$
$$\text{or } \partial\theta/\partial n = 1 \text{ (UHF) on solid walls} \tag{9b}$$

$$U = U_w = -Re_w/Re \quad V = W = 0 \quad \theta = 1 \text{ (UWT)}$$
$$\text{or } \partial\theta/\partial n = 1 \text{ (UHF) on porous wall} \tag{9c}$$

where n denotes the dimensionless outward normal direction to the duct wall. After the developing velocity and temperature fields along axial direction in the developing region are obtained, the computations of the peripherally averaged friction factor and Nusselt number are of practical interest. Following the usual definition, the expression for the product of the peripherally averaged friction factor and Reynolds number can be written based on the axial velocity gradient on the duct walls:

$$fRe = -2(\overline{\partial W/\partial n})_w. \tag{10}$$

Similarly, the peripherally averaged Nusselt number Nu can also be evaluated from the average temperature difference between the heated duct walls and the bulk fluid:

$$Nu = \overline{\partial\theta/\partial n}/(\overline{\theta_w-\theta_b}) \tag{11}$$

where the overbar means average around the perimeter. The bulk fluid temperature θ_b is defined as

$$\theta_b = \int_o^{(1+\gamma)/(2\gamma)}\int_o^{(1+\gamma)/2}\theta\cdot W\,\mathrm{d}X\,\mathrm{d}Y\Big/\int_o^{(1+\gamma)/(2\gamma)}\int_o^{(1+\gamma)/2} W\,\mathrm{d}X\,\mathrm{d}Y. \tag{12}$$

Governing parameters

As was noted above, the problem under consideration is governed by the following non-dimensional groups: wall Reynolds number Re_w, rotational Grashof number Gr_Ω, rotation number Ro, inlet Reynolds number Re, cross-sectional aspect ratio γ, dimensionless distance from inlet to axis of rotation Z_o and Prandtl number Pr. To conveniently discuss the effects of wall transpiration and rotation-induced buoyancy on mixed convection flow and heat transfer, the Z_o is fixed to be 50 ($Z_o = 50$) and the Prandtl number $Pr = 0.7$ for air is used in the computations. While the other parameters are then selected systematically to examine their influences on the characteristics of fluid flow and heat transfer. In this study, the wall Reynolds number Re_w measures the importance of the wall-transpiration effect. The rotational Grashof number Gr_Ω characterizes the significance of the rotation-induced buoyancy effect. The rotation number Ro represents the relative importance of the Coriolis force to the inertia force or the relative significance of the Coriolis-induced secondary flow to the forced flow effect. The cross-section aspect ratio γ is a geometric parameter. The flow characteristics may

be significantly influenced by the change in aspect ratio.

SOLUTION METHOD

In view of the impossibility of obtaining an analytic solution, the problem defined by the foregoing equations was solved by finite-difference procedures. In the present work, a numerical finite-difference scheme based on the vorticity–velocity method is used to obtain the solution of equations (3)–(7). The Du Fort–Frankel method [36] is employed in the axial direction and a central difference is used in the cross sections of equations (3)–(7). In this work, M and N grid points are uniformly distributed in the X and Y directions, respectively. Additionally, axial step sizes ΔZ are smaller near the entrance to account for the uneven variations of velocity and temperature. The detailed computation procedure for the simultaneous solutions is similar to that of Yan [34], modified to include the rotation-induced buoyancy effects.

A numerical experiment for the case of $Re_w = 10$, $Gr_\Omega = 2.5 \times 10^3$, $Ro = 0.05$, $Re = 1500$ and $\gamma = 1$ for UWT case was made to determine the grid spacing and axial step size required for acceptable accuracy. It was found that in the separate numerical runs that the deviations in Nu calculated with either $M \times N = 41 \times 41$ or 51×51 ($\Delta Z = 0.01 \sim 0.05$) are always within 3%. Furthermore, the deviations in Nu calculated using either $M \times N$ (ΔZ) $= 41 \times 41$ ($0.002 \sim 0.05$) or 41×41 ($0.01 \sim 0.05$) are all less than 1%. Accordingly, the computations involving a $M \times N$ (ΔZ) $= 41 \times 41$ ($0.01 \sim 0.05$) grid are considered to be sufficiently accurate to describe the mixed convection flow and heat transfer in radially rotating rectangular ducts with wall-transpiration effects. As a partial verification of the computational procedure, results were initially obtained for convection heat transfer in a radially rotating rectangular duct without wall transpiration effect. The results for Nusselt number and friction factor were compared with those by Jen *et al.* [28] and Fann and Yang [30]. The Nusselt number and friction factor were found to agree within 2%. In addition, the hydrodynamically developing flow in a stationary duct was calculated. The results are compared with those of Shah and London [37]. The differences in the apparent friction factor are within 1% at all axial locations. The above numerical tests indicate that the solution procedure adopted is suitable for the present study.

RESULTS AND DISCUSSION

Figure 2(a) shows a series of velocity vector distributions at $Gr_\Omega = 2.5 \times 10^3$, $Ro = 0.05$ and $Re = 1500$ in a square duct ($\gamma = 1$) with $Re_w = 0$ for the UWT case. Each vector is composed of the velocity components in the x and y directions, respectively. In the inlet region ($Z = 0.208$), flow resistance is larger near the duct walls, and hence fluid moves toward the so-called hydrodynamic center. As the fluid proceeds downstream, the rotational effects become important. A pair of symmetrical vortices are induced and circulate from the trailing wall ($X = 0$) to leading wall ($X = 1$) along the side walls ($Y = 0$ and 1) and return from the leading to trailing walls along the duct centerline ($Y = 0.5$). The vortex-pair continuously evolves as the fluid moves downstream. At $Z = 32.0$, a relatively weak second pair of vortices appears on the trailing wall ($X = 0$). Further downstream ($Z = 40$), the second pairs of vortices continue to grow.

Wall transpiration effects on the velocity vector distributions are depicted in Fig. 2(b). Comparison of the corresponding cross-flow patterns in Fig. 2(a) and (b) discloses that near the entrance, the so-called hydrodynamic center moves toward the porous wall ($X = 0$). Moreover, the second pairs of vortices on the trailing wall disappear due to the wall-transpiration effects.

The developing axial velocity profiles along the centerline $Y = 0.5$ for the UWT and UHF cases are depicted in Fig. 3(a) and (b) at various axial locations, respectively. It is well known that the axial velocity profiles for purely forced convection without rotation effect are symmetric with respect to the middle plane of $X = 0.5$. Once rotation is initiated, due to the Coriolis force, all the developing W profiles shift toward the trailing wall. An overall inspection on the dashed curves ($Re_w = 0$) reveals that near the entrance the velocity profile (curve A) is fairly uniform over the cross section. As the flow develops (curve B), the velocity in the core region is accelerated due to the entrance effect. As the flow proceeds downstream, the core is further accelerated and reduced in size and its peak axial velocity shifts farther toward $X = 0$, as shown in curves C–E. This is clearly due to the onset of second pair of counter-rotating vortices near the trailing wall, as shown in Fig. 2. This second pair of vortices would push the peak axial velocity toward the trailing wall. Note that the axial velocity gradient on the trailing wall ($X = 0$) is larger than that on the leading wall ($X = 1$). This implies that the friction factor on the trailing wall is larger than that on the leading wall. Comparison of solid and dashed curves indicates that near the inlet, the suction effect is negligibly small. But as the fluid moves away from the inlet, the effect of suction becomes more apparent. Additionally, the peak axial velocity for the solid curves is smaller from curves D–E due to the wall-transpiration effects. The effects of thermal boundary conditions on the developing W profiles can be found by comparing Fig. 3(a) and (b). It is apparent that smaller peak axial velocity is observed for the UHF case. This is due to a larger buoyancy-retarding effect for the UHF case.

The developments of temperature profiles along the centerline ($Y = 0.5$) for $Gr_\Omega = 2.5 \times 10^3$, $Ro = 0.05$, $Re = 1500$ and $\gamma = 1$ are presented in Fig. 3(c) and (d). For the UWT case in Fig. 3(c), a shift in the axial velocity toward the trailing wall ($X = 0$) results in a

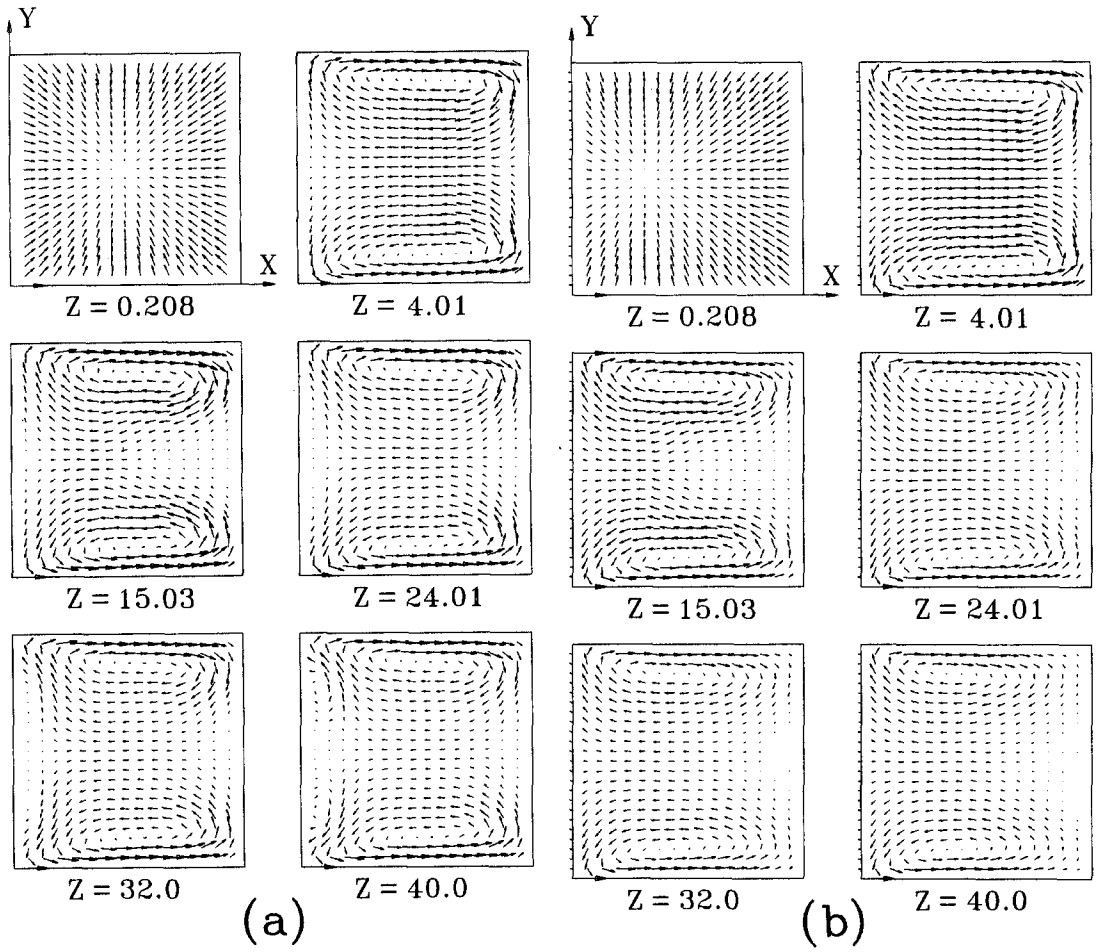

Fig. 2. Developments of velocity vector for (a) $Re_w = 0$; (b) $Re_w = 15$.

smaller shift in the temperature profiles. It is also interesting to observe that both the dashed and solid curves develop in a similar fashion. Careful inspection, however, discloses that the solid curves ($Re_w = 15$) develop a little more rapidly than the dashed curves ($Re_w = 0$) do. For the results of UHF in Fig. 3(d), a smaller temperature rise along the trailing wall ($X = 0$) results owing to the rotation effects. This is the mechanism of heat transfer enhancement on the trailing wall and heat transfer degradation on the leading wall due to rotation. A comparison of solid and dashed curves in Fig. 3(d) shows that in the presence of wall transpiration, the trailing wall temperature is reduced. But on the leading wall, the wall temperature is raised. This is due to the fact that the wall transpiration attracts a large portion of the mass to flow in a narrow region near the porous wall ($X = 0$) from which the fluid is being sucked. Therefore, the heat transfer along the porous wall is enhanced, which in turn, causes a small temperature rise along the trailing wall.

Figure 4 presents the axial variations of the peripherally averaged friction factor fRe and Nusselt number Nu with wall Reynolds number Re_w as a parameter. For comparison's purpose, both the results of UWT and UHF are presented. In Fig. 4, the suction effect is negligible up to a certain axial length Z. This axial distance depends primarily on the magnitude of the wall Reynolds number Re_w. The greater Re_w is, the shorter this distance is. A further investigation reveals that the curves branch out from the results of $Re_w = 0$, and after reaching a local minimum value, the curves increase. The occurrence of the first minimum in fRe or Nu is the appearance of the principal pair of vortices [30]. It should be noted that for the UHF case, the fRe and Nu curves for $Re_w = 20$ terminate at $Z = 35.5$ due to the flow reversal. In Fig. 4(a), the suction at the porous wall increases the fRe at the inlet section but decreases it further downstream. This is due to the fact that the wall transpiration attracts a large portion of the flowing mass to flow in a narrow region near the porous wall from which the fluid is being sucked. Therefore, the velocity gradient in this region increases, and, consequently, so does the fRe. However, as the flow proceeds in the axial direction, the total mass of the gas stream

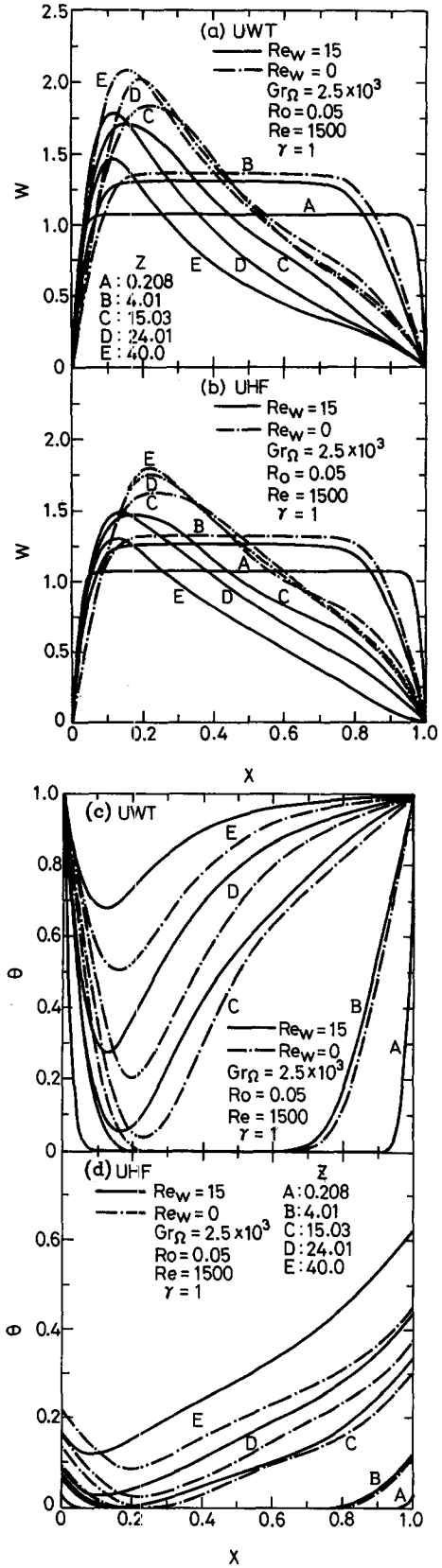

Fig. 3. Developments of axial velocity profiles and temperature profiles at $Y = 0.5$.

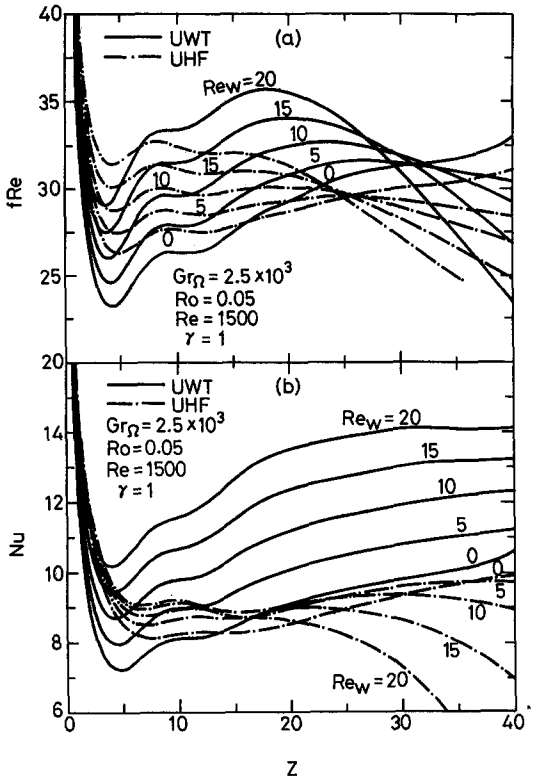

Fig. 4. Effects of Re_w on the variations of peripherally averaged friction factor and Nusselt number for $\gamma = 1$.

decreases due to the mass extraction, and hence the velocity gradient diminishes. This explains the reduction in the fRe in the downstream region. It is observed in Fig.4(b) that near the inlet, the Nu for UWT is lower than that for UHF. This is agreement with the stationary ducts in which the UHF case has higher heat transfer performance than the UWT case. As the flow proceeds downstream, however, the peripherally averaged Nu for the UWT case surpasses that for the UHF case. For UWT case, after the local minimum value, the Nu increases with the axial distance due to the effects of Coriolis force and wall suction. In addition, a larger Nu results for a larger Re_w. This is owing to the fact that wall suction changes the flow rate with the axial distance which has a hydrodynamic effect on the convective heat transfer. That is, the difference between wall temperature and bulk temperature is smaller for a larger wall suction, and hence the Nusselt number is larger for a higher Re_w.

In high rotation rate and/or high wall heat flux in rotating ducts, the centrifugal force may play a very critical role in the flow and heat transfer characteristics. Hence, it is interesting to examine the centrifugal buoyancy on the local fRe and Nu. Figure 5 presents the effects of rotational Grashof number Gr_Ω on the fRe and Nu with $Re_w = 10$, $Ro = 0.05$, $Re = 1500$ and $\gamma = 1$. It is found that the rotational Grashof number diminishes the Nusselt number. And the extent of retardation in Nu increases with Gr_Ω.

This decrease of heat transfer performance due to axial centrifugal buoyancy is expected because for a radially rotating outward flow the centrifugal buoyancy retards the heated air flow near the duct walls. This trend agrees with that proposed by Morris and Ayhan [18] and Han and Zhang [25]. It is also found in the separate numerical runs that the adverse effect of the Gr_Ω tends to diminish as the Reynolds number increases. In Fig. 5(a), the effects of centrifugal buoyancy on the fRe are relatively more complicated. Near the inlet, a larger fRe is experienced for a system with a smaller Gr_Ω. But as the flow moves downstream, the reverse trend is found. It is worth noting by comparing the solid and dashed curves that except the results near the entrance, the UWT case has higher fRe and Nu than the UHF case.

The effects of rotation number Ro on the peripherally averaged friction factor fRe and Nusselt number Nu are presented in Fig. 6(a) and (b), respectively, with $Re_w = 10$, $Gr_\Omega = 2.5 \times 10^3$, $Re = 1500$ and $\gamma = 1$. In these two subplots, the Coriolis force effect is insignificant near the inlet. At about $Z = 1.5$ or later, the Coriolis force becomes important and each curve branches out from the curve of $Ro = 0$ and $Gr_\Omega = 0$ and after reaching a local minimum value, the curve increases. The occurrence of the first minimum in fRe and Nu is due to the combined entrance and Coriolis force effects. It is worth noting that for $Ro = 0.075$ and 0.1, oscillations in the variations of

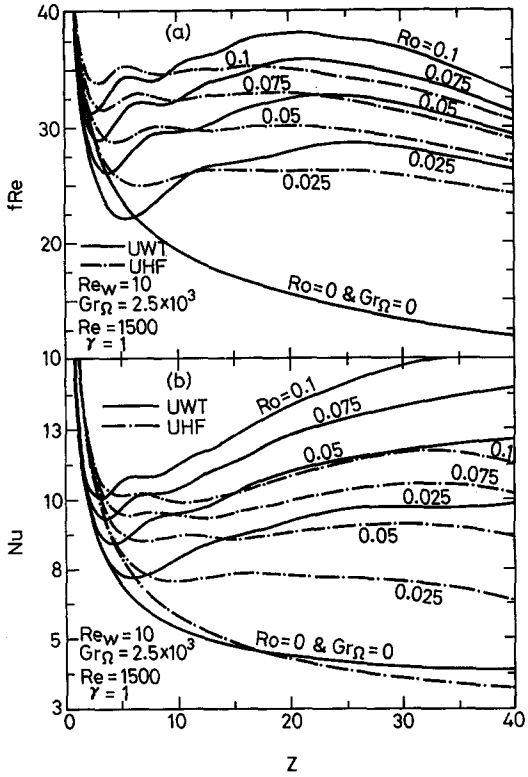

Fig. 6. The variations of the peripherally averaged friction factor and Nusselt number with Ro as parameter for $\gamma = 1$.

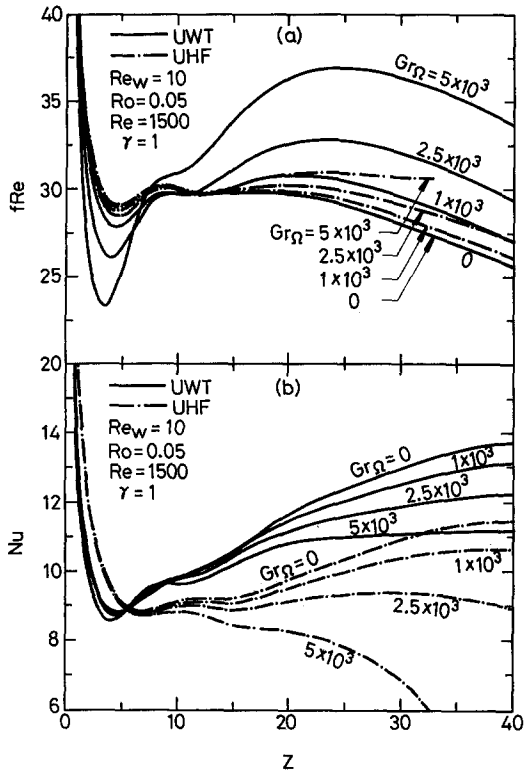

Fig. 5. Effects of Gr_Ω on the variations of peripherally averaged friction factor and Nusselt number for $\gamma = 1$.

fRe and Nu exist after the first local minimum. This behavior is due to the emergence and decay of the second pair of vortices near the trailing wall. The similar trend is also found by Fann and Yang [30] for rotating heat transfer without wall-transpiration effects. In addition, larger fRe and Nu are observed for a system with a larger Ro due to the stronger Coriolis force. In the separate numerical runs, it was found that larger fRe and Nu are noted for a system with a higher inlet Reynolds number Re due to a larger forced convection effect.

In rotating ducts the cross-section aspect ratio γ may affect the strength of secondary flow. Therefore, the effects of the channel aspect ratio γ, on the friction factor fRe and Nusselt number Nu are of practical interest. The axial variations of fRe and Nu for aspect ratios $\gamma = 2$ and 0.5 are shown in Figs. 7 and 8, respectively, with wall Reynolds number Re_w as a parameter. The fRe values are higher in the flatter rectangular duct ($\gamma = 2$) and lower in the narrower rectangular ducts ($\gamma = 0.5$) compared with those in the square duct in Fig. 4. It is also found that the wall-transpiration effect is relatively significant for a system with a small γ. This is due to the fact that a channel with a smaller γ is a channel with a wider trailing wall (i.e. porous wall), which in turn causes a significant suction effect.

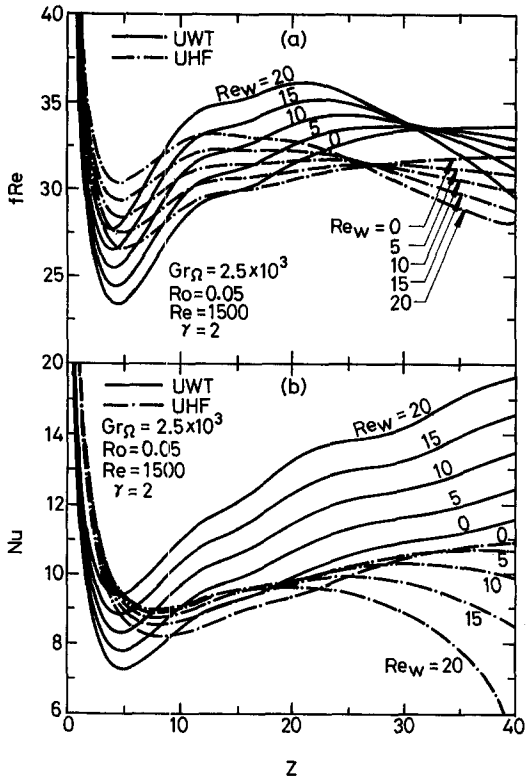

Fig. 7. The variations of the peripherally averaged friction factor and Nusselt number with Re_w as parameter for $\gamma = 2$.

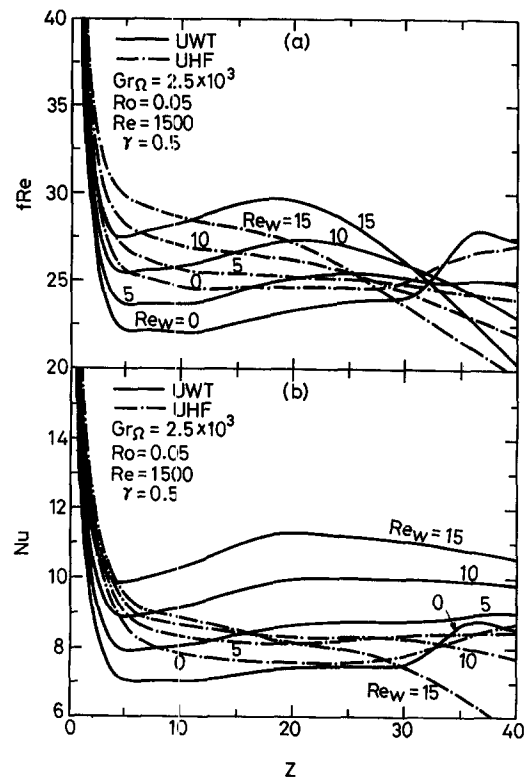

Fig. 8. The variations of the peripherally averaged friction factor and Nusselt number with Re_w as parameter for $\gamma = 0.5$.

CONCLUSIONS

The problem of mixed convection flow and heat transfer in radially rotating rectangular ducts with wall-transpiration and rotation-induced buoyancy effects has been studied numerically. A relatively novel vorticity–velocity method successively solved the three-dimensional parabolic governing equations. The effects of the wall Reynolds number Re_w, rotational Grashof number Gr_Ω, rotation number Ro, aspect ratio γ, and thermal boundary conditions on the flow and heat transfer are examined in detail. The major conclusions of this work are as follows:

(1) The variations of the peripherally averaged friction factor fRe and Nusselt number Nu show that the effects of the rotation and the wall-transpiration are negligible up to a certain entry length, Z, which depends primarily on the magnitude of the rotation number, Ro, and wall Reynolds number, Re_w. The distributions of fRe and Nu are characterized by a decay near the entrance due to the entrance effect; but the decay is attenuated by the onset of secondary flow.

(2) For both UWT and UHF cases, near the entrance, the fRe increases with Re_w. But as the fluid move downstream, the fRe decreases with Re_w.

(3) For UWT case, a larger Nu is noted for a system with a greater wall-transpiration effect (Re_w). But for UHF case, the wall suction effect is complicated. The Nu near the inlet increases with an increase in the wall Reynolds number Re_w, but the trend is reversed as the fluid proceeds downstream.

(4) The centrifugal buoyancy decreases the heat transfer performance and the extent of retardation in Nu increases with Gr_Ω.

(5) The smaller suction effects on circumferentially averaged fRe and Nu are observed for a rectangular duct with a larger value of aspect ratio ($\gamma = 2$) due to the relatively narrower porous wall.

(6) The peripherally averaged fRe and Nu for the UWT case are lower than those for the UHF case near the inlet but surpass them downstream.

Acknowledgement—The financial support of this research by the National Science Council, R.O.C., under the contract NSC 82-0401-E211-016 is greatly appreciated.

REFERENCES

1. D. K. Hennecks, Heat transfer problems in aero-engines. In *Heat and Mass Transfer in Rotating Machinery* (edited by D. E. Metzger and N. H. Afgan), pp. 353–379. Hemisphere, New York (1984).
2. C. Y. Soong, Transport phenomena in porous-walled ducts—a review, *Proceedings of the First National Conference on Science and Technology of National Defence*, Taiwan, R.O.C., pp. 241–249 (1992).
3. A. S. Berman, Laminar flow with porous walls, *J. Appl. Phys.* **24**, 1232–1235 (1953).
4. P. L. Donoughe, Analysis of laminar incompressible flow in semi-porous channels, NASA TN3759, NACA (1956).
5. G. D. Raithby and D. C. Knudsen, Hydrodynamic development in a duct with suction and blowing, *J. Appl. Mech.* **96**, 896–902 (1974).

6. M. M. Sorour, M. A. Hassab and S. Estafanous, Developing laminar flow in a semiporous two-dimensional channel with nonuniform transpiration, *Int. J. Heat Fluid Flow* **8,** 44–54 (1987).
7. L. F. Carter and W. N. Gill, Asymptotic solution for combined free and forced convection in vertical and horizontal conduits with uniform suction and blowing, *A.I.Ch.E. J.* **10,** 330–339 (1964).
8. R. M. Terrill, Heat transfer in laminar flow between parallel porous plates, *Int. J. Heat Mass Transfer* **8,** 1491–1497 (1965).
9. R. B. Kinney, Fully developed frictional and heat transfer characteristics of laminar flow in porous tubes, *Int. J. Heat Mass Transfer* **11,** 1393–1401 (1968).
10. R. J. Pederson and R. B. Kinney, Entrance-region heat transfer for laminar flow in porous tubes, *Int. J. Heat Mass Transfer* **14,** 159–161 (1971).
11. G. D. Raithby, Laminar heat transfer in the thermal entrance region of circular tubes and two-dimensional rectangular ducts with wall suction and injection, *Int. J. Heat Mass Transfer* **14,** 224–243 (1971).
12. J. R. Doughty and H. C. Perkins, Jr, Variable properties laminar gas flow heat transfer in the entry region of parallel porous plates, *Int. J. Heat Mass Transfer* **16,** 663–668 (1973).
13. S. J. Rhee and D. K. Edwards, Laminar entrance flow in a flat plate duct with asymmetric suction and heating, *Numer. Heat Transfer* **4,** 85–100 (1981).
14. A. Fagher, Heat-transfer characteristics in annuli with blowing or suction at the walls, *J. Thermophys. Heat Transfer* **4,** 59–66 (1990).
15. G. J. Hwang, Y. C. Cheng and M. L. Ng, Developing laminar flow and heat transfer in a square duct with one-walled injection and suction, *Int. J. Heat Mass Transfer* **36,** 2429–2440 (1993).
16. Y. Mori and W. Nakayama, Convective heat transfer in a rotating radial circular pipe (1st report, laminar region), *Int. J. Heat Mass Transfer* **11,** 1025–1040 (1968).
17. G. J. Hwang and T. C. Jen, Convective heat transfer in rotating isothermal ducts, *Int. J. Heat Mass Transfer* **33,** 1817–1828 (1990).
18. W. D. Morris and T. Ayhan, Observation on the influence of rotation on heat transfer in the coolant channel of gas turbine rotor blade, *Proc. Inst. Mech. Engrs* **193,** 303–311 (1979).
19. W. D. Morris, *Heat Transfer and Fluid Flow in Rotating Coolant Channels*. Wiley, New York (1981).
20. R. Siegel, Analysis of buoyancy effect on fully developed laminar heat transfer in a rotating tube, *ASME J. Heat Transfer* **107,** 338–344 (1985).
21. S. P. Harasgama and W. D. Morris, The influence of rotation on the heat transfer characteristics of circular, triangular, and square-sectioned coolant passages of gas turbine rotor blades, *ASME J. Turbomachinery* **110,** 44–50 (1988).
22. C. Y. Soong, S. T. Lin and G. J. Hwang, An experimental study of convective heat transfer in radially rotating rectangular ducts, *J. Heat Transfer* **113,** 604–611 (1991).
23. J. H. Wagner, B. V. Johnson and T. J. Hajek, Heat transfer in rotating passages with square smooth walls and radial outward flow, *J. Turbomachinery* **113,** 42–51 (1991).
24. M. E. Taslim, L. A. Bondi and DM. Kercher, An experimental investigation of heat transfer in an orthogonally rotating channel roughened with 45 deg criss-cross ribs on two opposite walls, *ASME J. Turbomachinery* **113,** 346–353 (1991).
25. J. C. Han and Y. M. Zhang, Effect of uneven wall temperature on local heat transfer in a rotating square channel with smooth walls and radial outward flow, *J. Heat Transfer* **114,** 850–858 (1992).
26. J. H. Wanger, B. V. Johnson and F. C. Kopper, Heat transfer in rotating serpentine passage with smooth walls, *J. Turbomachinery* **113,** 321–330 (1991).
27. S. Fann, W. J. Yang and N. Zhang, Local heat transfer in a rotating serpentine passage with rib-roughened surface, *Int. J. Heat Mass Transfer* **37,** 217–228 (1994).
28. T. C. Jen, A. S. Lavine and G. J. Hwang, Simultaneously developing laminar convection in rotating isothermal square channels, *Int. J. Heat Mass Transfer* **35,** 239–254 (1992).
29. T. C. Jen and A. S. Lavine, Laminar heat transfer and fluid flow in the entrance region of a rotating duct with rectangular cross section: the effect of aspect ratio, *J. Heat Transfer* **114,** 574–581 (1992).
30. S. Fann and W. J. Yang, Hydrodynamically and thermally developing laminar flow through rotating channel having isothermal walls, *Numer. Heat Transfer A* **22,** 257–288 (1992).
31. S. Fann, W. J. Yang and S. Mochizuki, Transport phenomena at entrance regions of rotating heated channels with laminar throughflow, *ASME J. Heat Transfer* **116,** 239–242 (1994).
32. C. Y. Soong and G. J. Hwang, Laminar mixed convection in a radially rotating semiporous channel, *Int. J. Heat Mass Transfer* **33,** 1805–1816 (1990).
33. C. Y. Soong and G. J. Hwang, Effects of stress work on similarity solutions of mixed convection in rotating channel with wall-transpiration, *Int. J. Heat Mass Transfer* **36,** 845–856 (1993).
34. W. M. Yan, Developing flow and heat transfer in radially rotating rectangular ducts with wall-transpiration effects, *Int. J. Heat Mass Transfer* **37,** 1465–1473 (1994).
35. S. V. Patankar and D. B. Spalding, A calculation procedure for heat, mass and momentum transfer in three-dimensional parabolic flows, *Int. J. Heat Mass Transfer* **15,** 1787–1806 (1972).
36. P. J. Roache, *Computational Fluid Dynamics*, pp. 61–64. Reinhold, New York (1971).
37. R. A. Shah and A. L. London, *Laminar Flow Forced Convection in Ducts*, Suppl. 1 to Adv. Heat Transfer, pp. 196–222. Academic Press, New York (1978).